Available online at www.sciencedirect.com
ScienceDirect
Journal of the Mechanics and Physics of Solids 56 (2008) 1534–1553
JOURNAL OF THE MECHANICS AND PHYSICS OF SOLIDS
www.elsevier.com/locate/jmps

A computational method for dislocation–precipitate interaction

Akiyuki Takahashi[a,*], Nasr M. Ghoniem[b]

[a]*Department of Mechanical Engineering, Faculty of Science and Technology, Tokyo University of Science, 2641 Yamazaki, Noda-shi, Chiba 278-8510, Japan*

[b]*Department of Mechanical and Aerospace Engineering, University of California, Los Angeles, Los Angeles, CA 90095, USA*

Received 10 April 2007; received in revised form 31 July 2007; accepted 2 August 2007

Abstract

A new computational method for the elastic interaction between dislocations and precipitates is developed and applied to the solution of problems involving dislocation cutting and looping around precipitates. Based on the superposition principle, the solution to the dislocation–precipitate interaction problem is obtained as the sum of two solutions: (1) a dislocation problem with image stresses from interfaces between the dislocation and the precipitate, and (2) a correction solution for the elastic problem of a precipitate with an initial strain distribution. The current development is based on a combination of the parametric dislocation dynamics (PDD) and the boundary element method (BEM) with volume integrals.The method allows us to calculate the stress field both inside and outside precipitates of elastic moduli different from the matrix, and that may have initial coherency strain fields. The numerical results of the present method show good convergence and high accuracy when compared to a known analytical solution, and they are also in good agreement with molecular dynamics (MD) simulations. Sheared copper precipitates (2.5 nm in diameter) are shown to lose some of their resistance to dislocation motion after they are cut by leading dislocations in a pileup. Successive cutting of precipitates by the passage of a dislocation pileup reduces the resistance to about half its original value, when the number of dislocations in the pileup exceeds about 10. The transition from the shearable precipitate regime to the Orowan looping regime occurs for precipitate-to-matrix elastic modulus ratios above approximately 3–4, with some dependence on the precipitate size. The effects of precipitate size, spacing, and elastic modulus mismatch with the host matrix on the critical shear stress (CSS) to dislocation motion are presented.

Keywords: Dislocations; Precipitates; Boundary integral equations; Strength; Metallic materials

1. Introduction

Alloy design requires optimization of many, and often conflicting requirements, such as strength, ductility, corrosion resistance, etc. Phase transformations are at the heart of the tools available to create desirable microstructure, and hence engender optimized properties. For example, the strength of steels can be varied from several hundred MPa to over 2 GPa by appropriate heat treatments, composition control, precipitate strengthening, and cold-working. Precipitation strengthening is one of the most effective techniques to design

*Corresponding author. Tel.: +81 4 7124 1501.
E-mail address: takahash@me.noda.tus.ac.jp (A. Takahashi).

0022-5096/$ - see front matter © 2007 Elsevier Ltd. All rights reserved.
doi:10.1016/j.jmps.2007.08.002

advanced alloys with superior strength characteristics. However, excessive strengthening may lead to loss of ductility and plastic flow localization. The mechanism is based on blocking the motion of dislocations by second phase precipitates that are dispersed in the alloy's matrix, and thus results in significant improvements in the yield strength and hardness of the alloy. It is therefore essential that the interaction between dislocations and precipitates is accurately and efficiently modeled in order to explore the basic physics of these interactions and to enable rational alloy design.

When dislocations approach precipitates, they experience attraction/repulsion forces that can significantly retard their motion. Such forces result from a number of factors: (1) mismatch between the elastic properties of the matrix and precipitate; (2) coherency strains between the precipitate and matrix; (3) misfit dislocations at incoherent precipitate–matrix interfaces; and (4) changes in the core structure of dislocations as they penetrate precipitates. In practice, however, not all these factors exist simultaneously, and one or several of them are utilized for strengthening. We will focus here on the influence of the first two factors on precipitation strengthening. The key parameter in understanding the physics of dislocation–precipitate interaction is the critical stress required to move a dislocation past a distribution of precipitates, either by cutting through them or by looping around them (the Orowan mechanism). The parameters that determine the critical stress are: the precipitate shape, elastic constants, crystal structure, and spacing between precipitates.

Friedel developed a statistical model to evaluate the critical shear stress of metals with randomly distributed precipitates (Friedel, 1964). He introduced an effective spacing between precipitates, which is a function of the critical shear stress, the volume fraction of the precipitate, the Burgers vector of the dislocation and the self-force on the dislocation. The critical shear stress is evaluated with the effective spacing and the maximum force in the interaction between the dislocation and the precipitate. On the other hand, Nembach studied the effect of the difference in the elastic shear modulus between a spherical precipitate and the matrix on the maximum force in the interaction with a straight dislocation, and found that the critical shear stress is proportional to $\Delta\mu^{1.5}$ and $r_p^{0.22}$, where $\Delta\mu$ is the modulus difference and r_p is the radius of the spherical precipitate (Nembach, 1983). Fleischer also gave an equation to calculate the maximum force in the interaction between a straight edge dislocation and a solute atom (Fleischer, 1961, 1963). However, in all these attempts, the shape of the dislocation is restricted to straight, and the precipitate to be spherical or ellipsoidal. During a dynamic interaction process, dislocations can re-configure in complex curved shapes that frequently change during the interaction process. Moreover, precipitates are not generally spherical or ellipsoidal. In the present work, we remove all these restrictions and develop an efficient computational method to resolve the detailed interaction physics.

Recently, computer simulations to investigate the dynamics of dislocation ensembles (based on the method of dislocation dynamics (DD)), have been developed and successfully applied to the study of many aspects of the metal plasticity (Devincre and Kubin, 1994; Zbib et al., 1998; Schwarz, 1999; Ghoniem et al., 2000; Wang et al., 2001; Xiang et al., 2003). One of the advantages of DD simulations in comparison with analytical approaches is the ability to deal with flexible dislocations with complex shapes. van der Giessen and Needleman (1995) introduced boundary conditions to treat free surfaces and cracks into DD simulations using the superposition principle and the finite element method (FEM). Shin et al. (2003, 2005) applied the idea of the superposition principle to dislocation–impenetrable precipitate interaction problems, and studied the effect of the elastic constant mismatch between the precipitate and the matrix on the critical shear stress for the Orowan mechanism using DD and FEM. However, and up till now, no method has been advanced for the interaction between dislocations and penetrable precipitates in the most general sense (i.e. different elastic constants, coherency strains, etc.).

The objective of the present study is to develop a computational method for solving dislocation–precipitate interaction problems based on linear elasticity theory, which enables us to investigate the interaction between flexible dislocations and penetrable precipitates. Based on the superposition principle, the solution for the dislocation–precipitate interaction problem can be obtained as the sum of the solutions to two different problems: (1) a dislocation with image stresses from interfaces between precipitates and the matrix, and (2) a precipitate problem with initial stresses, which result from the elastic constants mismatch between the precipitate and the matrix and the *eigen* strain in the precipitate. The dislocation problem is solved here by the parametric dislocation dynamics (PDD) method (Ghoniem et al., 2000). For the precipitate problem with initial stresses, a boundary integral equation is formulated and solved by the boundary element method

(BEM). The accuracy of the method will be confirmed by comparing the numerical results to a known solution of the image stress attributed to the interaction between a screw dislocation and a spherical precipitate. Also, the consistency of the results of the present method with the results of a corresponding atomistic molecular dynamics (MD) method is examined. Finally, the present method is applied to investigations of the critical shear stress (CSS) of precipitates slipped by dislocation cuttings, and with different diameters, spacings and elastic constants.

The paper is organized as follows. First, an inhomogeneous inclusion problem with dislocations, which is the most general description of the precipitate problem, is defined and represented as a sum of two different problems based on the superposition principle in Section 2. The computational methods to solve the two problems are presented in Section 3. Numerical convergence and accuracy of the present method and the consistency of the results with MD simulations are examined in Section 4. The CSS of multiply-cut precipitates is investigated in Section 5.1. The effects of the diameter, spacing and elastic constants mismatch on the CSS are then investigated in Section 5.2. Finally, discussions and conclusions are given in Section 6.

2. Inhomogeneous inclusions and dislocations

The term "inhomogeneous inclusion" is used to describe the situation where an eigen strain ε_{ij} is prescribed in a finite sub-domain Ω within a body D, and is zero in the matrix $D-\Omega$, and the domain Ω has different elastic properties from the matrix D. In this case, Ω is called an inhomogeneous inclusion, or simply an inhomogeneity. Inhomogeneous inclusions can be considered as the most general description of coherent precipitates. Let us consider N_p inhomogeneous inclusions with eigen strains ε^m_{ij} and elastic constants C^m_{ijkl} in an infinite body with elastic constants C_{ijkl}. The superscript m denotes the mth inhomogeneous inclusion. The infinite body D contains an arbitrary number of dislocations, and is subjected to an external stress σ^0_{ij} at infinity. Following Mura (1982), we describe the stress in $D-\Omega$ as

$$\sigma^0_{ij}+\sigma_{ij}=C_{ijkl}(\varepsilon^0_{kl}+\varepsilon_{kl}) \quad \text{in } D-\Omega, \tag{1}$$

where, $\varepsilon^0_{ij}=C^{-1}_{ijkl}\sigma^0_{kl}$, ε_{ij} is the strain produced by dislocations and the external stress σ^0_{ij}. The domain Ω contains the total volume of N_p inhomogeneous inclusions (precipitates). Similarly, the stress in the mth inhomogeneous inclusion Ω^m can also be defined as

$$\sigma^0_{ij}+\sigma_{ij}=C^m_{ijkl}(\varepsilon^{m,0}_{kl}+\varepsilon^m_{kl}-\varepsilon^m_{kl}) \quad \text{in } \Omega^m, \tag{2}$$

where $\varepsilon^{m,0}_{ij}=C^{m,-1}_{ijkl}\sigma^0_{kl}$. Eshelby (1957) gave an analytical solution to an inhomogeneous inclusion problem by the equivalent inclusion method. However, application of his solution is limited only to cases where the shape of the inhomogeneous inclusion is an ellipsoid, and the prescribed strain field such as the eigen strain is uniformly distributed within the inhomogeneity. Therefore, we need an alternative and more general method to solve general inhomogeneous inclusion problems.

To treat boundary and interface problems, van der Giessen and Needleman (1995) have developed a hybrid of the DD and FEM techniques, and they again based the solution on the superposition principle. In their approach, there is no limitation on the shape of the inhomogeneous inclusion, and on the strain distribution. As shown in Fig. 1, using the superposition principle, the problem can be decomposed into two problems: (1) a dislocation problem in an infinite homogeneous body, and (2) a correction problem, which is an elastic problem of precipitates. At first, the stress field in the original inhomogeneous inclusion problem is decomposed into two parts for the dislocation and correction problems, as follows:

$$\sigma^0_{ij}+\sigma_{ij}=\tilde{\sigma}_{ij}+\hat{\sigma}_{ij} \quad \text{in } D, \tag{3}$$

where, $\tilde{\sigma}_{ij}$ and $\hat{\sigma}_{ij}$ are the stresses in the dislocation problem and in the correction problem, respectively. The stress in the dislocation problem $\tilde{\sigma}_{ij}$ is defined by

$$\tilde{\sigma}_{ij}=C_{ijkl}(\varepsilon^0_{kl}+\tilde{\varepsilon}_{kl}) \quad \text{in } D, \tag{4}$$

where $\tilde{\varepsilon}_{ij}$ is the strain produced by dislocations in D. The stress in the correction problem $\hat{\sigma}_{ij}$ can be obtained as the difference between the stresses in the original inhomogeneous inclusion and the dislocation problems,

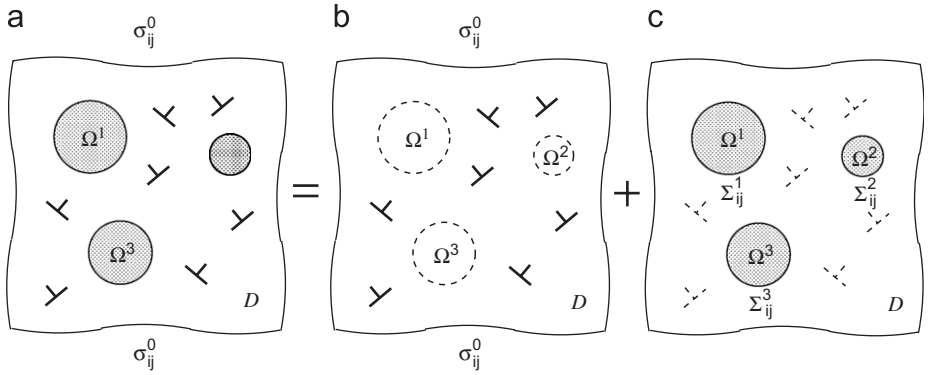

Fig. 1. Schematic for the dislocation–precipitate interaction problem with the superposition principle: (a) original problem; (b) the dislocation problem with image stresses; and (c) the correction (precipitate) problem with initial stresses Σ^m_{ij}.

which gives

$$\hat{\sigma}_{ij} = C_{ijkl}\hat{\varepsilon}_{kl} \quad \text{in } D - \Omega, \tag{5}$$

$$\hat{\sigma}_{ij} = C^m_{ijkl}\hat{\varepsilon}^m_{kl} - C^m_{ijkl}\varepsilon^m_{kl} + (C^m_{ijkl} - C_{ijkl})(\varepsilon^{m,0}_{kl} + \tilde{\varepsilon}_{kl}) \quad \text{in } \Omega^m. \tag{6}$$

For the sake of simplicity, Eq. (6) is rewritten as

$$\hat{\sigma}_{ij} = C^m_{ijkl}\hat{\varepsilon}^m_{kl} + \Sigma^m_{ij} \quad \text{in } \Omega^m, \tag{7}$$

where $\Sigma^m_{ij} = -C^m_{ijkl}\varepsilon^m_{kl} + (C^m_{ijkl} - C_{ijkl})(\varepsilon^{m,0}_{kl} + \tilde{\varepsilon}^m_{kl})$. From Eqs. (5) and (7), the correction solution can be considered as the solution to an inhomogeneity problem with an initial stress Σ^m_{ij}.

3. Computational method

Utilization of the FEM method to solve for the boundary correction problem in DD simulations has recently been proposed by a number of investigators (van der Giessen and Needleman, 1995; Shin et al., 2003, 2005; Gracie et al., 2007). Nevertheless, a number of difficulties arise in FEM-based methods, especially for 3D applications, as described below:

(1) The entire domain (volume) must be discretized into elements, while in the BEM-based method, only surfaces are discretized.
(2) Infinite domains cannot be modeled with finite elements, and special elements are to be developed.
(3) The stress between two neighboring elements is not continuous, because the elements used in FEM generally satisfy only the C^0 continuity conditions.

The first of these three difficulties is a significant impediment to the development of DD simulations involving a large number of inhomogeneous inclusions. To avoid the disadvantages associated with FEM-based boundary corrections in 3D DD simulations involving many precipitates, we develop here the BEM as an alternative. The BEM method requires only boundary discretization, which can greatly simplify the process of the mesh generation, deals easily with an infinite domain, and will be shown to be of the same form as the PDD method. The stress field calculated by the BEM method is also continuous everywhere in the domain.

3.1. The parametric dislocation dynamics

One of the main ingredients of the PDD method (Ghoniem et al., 2000) is to calculate the stress field within inhomogeneous inclusions induced by dislocation loops. In the PDD method, a dislocation loop of an arbitrary 3D shape is discretized into N_s curved parametric segments. For each segment j, we choose a set of generalized coordinates $q^{(j)}_{ik}$ and corresponding shape function $N_i(\omega)$ to represent the configuration of the

segment, that is

$$x_k^{(j)}(\omega) = \sum_i N_i(\omega) q_{ik}^{(j)}, \tag{8}$$

where $x_k^{(j)}$ is the Cartesian position of a point on segment j, and ω is a parameter with an interval $0 \leqslant \omega \leqslant 1$. In this study, we employ cubic spline segments, and then the shape functions $N_i(\omega)$ take the form

$$N_1(\omega) = 2\omega^3 - 3\omega^2 + 1, \quad N_2(\omega) = -2\omega^3 + 3\omega^2,$$

$$N_3(\omega) = \omega^3 - 2\omega^2 + \omega, \quad N_4(\omega) = \omega^3 - \omega^2. \tag{9}$$

In this case, the generalized coordinates $q_{ik}^{(j)}$ are the position and tangent vectors associated with the beginning and end nodes on segment j.

Let us assume that there are N_d dislocation loops, and each dislocation loop has N_s curved parametric segments. A stress at a point produced by curved dislocation loops can be calculated by the fast sum method (Ghoniem, 1999; Ghoniem and Sun, 1999), which is given by

$$\sigma_{ij} = \frac{\mu}{4\pi} \sum_{\gamma}^{N_\mathrm{d}} \sum_{\beta}^{N_\mathrm{s}} \sum_{\alpha}^{Q_\mathrm{max}} b_n w_\alpha \left[\frac{1}{2} R_{,mpp} (\varepsilon_{jmn} x_{i,\omega}^{(\beta)} + \varepsilon_{imn} x_{j,\omega}^{(\beta)}) + \frac{1}{1-\nu} \varepsilon_{kmn} (R_{,ijm} - \delta_{ij} R_{,ppm}) x_{k,\omega}^{(\beta)} \right], \tag{10}$$

where μ is the elastic shear modulus, ν is the Poisson's ratio, b_n is the n component of the Burgers vector, w_α is the weight in the standard Gaussian quadrature, and R is the magnitude of a relative position vector between a point $x_k^{(\beta)}$ on ω dislocation loop and a field point at which the stress is evaluated.

Once the dislocation stress field and the image stress is obtained, the PDD method enables us to simulate the dynamics of dislocation ensembles. A variational form of the governing equation of motion of a dislocation loop Γ is given by

$$\int_\Gamma (F_k - B_{\alpha k} V_\alpha) \delta r_k |\mathrm{d}\mathbf{s}| = 0, \tag{11}$$

where F_k is the force, $B_{\alpha k}$ is the resistivity matrix and V_k is the velocity. Further details of the PDD method can be found elsewhere (Ghoniem et al., 2000).

3.2. Boundary integral equations

Boundary integral equations for the correction problem are derived on the basis of a multi-zone BEM, which enables us to solve for the elastic field in a body containing domains with different elastic constants. For an inhomogeneous inclusion, Ω^m, the boundary conditions for the displacement $\bar{u}_i^m$ and traction $\bar{t}_i^m$ vectors are given by

$$\hat{u}_i^m = \bar{u}_i^m \quad \text{on } \Gamma_u^m,$$

$$\hat{t}_i^m = \hat{\sigma}_{ij} n_j^m = (C_{ijkl}^m \varepsilon_{kl}^m + \Sigma_{ij}^m) n_j^m = \bar{t}_i^m \quad \text{on } \Gamma_t^m, \tag{12}$$

where n_j^m is the unit outward vector normal to the surface of the mth inhomogeneous inclusion, and Γ_u^m and Γ_t^m are the boundaries of the mth inhomogeneous inclusion with the displacement and the traction boundary conditions, respectively. The boundary integral equation for the correction field is then written as

$$c_{ij}(P)\hat{u}_j^m(P) = \int_{\Gamma^m} U_{ij}^m(P,Q)\{\hat{t}_j^m(Q) - \Sigma_{jk}^m(Q) n_k^m(Q)\}\,\mathrm{d}\Gamma - \int_{\Gamma^m} T_{ij}^m(P,Q)\hat{u}_j^m(Q)\,\mathrm{d}\Gamma + \int_{\Omega^m} \Sigma_{jk,k}^m(q) U_{ij}^m(P,q)\,\mathrm{d}\Omega, \tag{13}$$

where c_{ij} is the coefficient matrix, which can generally be computed using the rigid body translation, and U_{ij}^m and T_{ij}^m are the kernel functions of displacement and traction defined with elastic constants of the mth

inhomogeneous inclusion, respectively. The volume integral term for the initial stress Σ_{ij}^m is found using integration by parts:

$$\int_{\Omega^m} \Sigma_{jk,k}^m(q) U_{ij}^m(P,q)\,\mathrm{d}\Omega = \int_{\Gamma^m} \Sigma_{jk}^m(Q) n_k^m(Q) U_{ij}^m(P,Q)\,\mathrm{d}\Gamma - \int_{\Omega^m} \Sigma_{jk}^m(q) U_{ij,k}^m(P,q)\,\mathrm{d}\Omega. \tag{14}$$

Substituting Eq. (14) into Eq. (13), we have

$$c_{ij}(P)\hat{u}_j^m(P) = \int_{\Gamma^m} U_{ij}^m(P,Q)\hat{\tilde{t}}_j^m(Q)\,\mathrm{d}\Gamma - \int_{\Gamma^m} T_{ij}^m(P,Q)\hat{u}_j^m(Q)\,\mathrm{d}\Gamma - \int_{\Omega^m} \Sigma_{jk}^m(q) U_{ij,k}^m(P,q)\,\mathrm{d}\Omega. \tag{15}$$

On the other hand, for an infinite body D with interfaces between an inhomogeneous inclusions Ω and the infinite body D, the boundary integral equation can be written as

$$c_{ij}(P)\hat{u}_j(P) = \int_{\Gamma} U_{ij}(P,Q)\hat{t}_j(Q)\,\mathrm{d}\Gamma - \int_{\Gamma} T_{ij}(P,Q)\hat{u}_j(Q)\,\mathrm{d}\Gamma. \tag{16}$$

Assuming that the infinite body and inhomogeneous inclusions are perfectly bonded, the displacements and the tractions on the interfaces between the infinite body and inhomogeneous inclusions must satisfy

$$\left.\begin{aligned} \hat{u}_j - \hat{u}_j^m &= 0 \\ \hat{t}_j + \hat{\tilde{t}}_j^m &= 0 \end{aligned}\right\} \quad \text{on } \Gamma^m. \tag{17}$$

Finally, substituting these conditions into Eq. (15), the boundary integral equation for the mth inhomogeneous inclusion takes the following form, with displacements and tractions defined on the surfaces surrounding each inclusion in the infinite body,

$$c_{ij}(P)\hat{u}_j(P) = -\int_{\Gamma^m} U_{ij}^m(P,Q)\hat{t}_j(Q)\,\mathrm{d}\Gamma - \int_{\Gamma^m} T_{ij}^m(P,Q)\hat{u}_j(Q)\,\mathrm{d}\Gamma - \int_{\Omega^m} \Sigma_{jk}^m(q) U_{ij,k}^m(P,q)\,\mathrm{d}\Omega. \tag{18}$$

Eqs. (16) and (18) are the final forms of the multi-zone BEM method for the correction field, and can be solved numerically to compute displacements and tractions on all interfaces. Once displacements and tractions on interfaces are obtained by solving the above boundary integral equations, the stresses at any point can be easily computed

$$\hat{\sigma}_{ij}(p) = \int_{\Gamma} D_{ijk}(p,Q)\hat{t}_k(Q)\,\mathrm{d}\Gamma - \int_{\Gamma} S_{ijk}(p,Q)\hat{u}_k(Q)\,\mathrm{d}\Gamma, \tag{19}$$

where

$$D_{ijk}(p,Q) = \tfrac{1}{2} C_{ijln}(U_{lk,n}(p,Q) + U_{nk,l}(p,Q)),$$

$$S_{ijk}(p,Q) = \tfrac{1}{2} C_{ijln}(T_{lk,n}(p,Q) + T_{nk,l}(p,Q)). \tag{20}$$

On the other hand, the stress inside an inhomogeneous inclusion cannot be accurately calculated even when the displacements and tractions on interfaces are known, because the volume integral term in Eq. (18) gives rise to a strong singularity in the stress computation. To solve the problem accurately and effectively, we resort again to the dislocation and correction problems, and consider the calculation of the stress field inside of the mth inhomogeneous inclusion. In this case, the dislocation problem is defined in an infinite body D with the elastic constants of the mth inhomogeneous inclusion:

$$\tilde{\sigma}_{ij} = C_{ijkl}^m(\varepsilon_{kl}^{m,0} + \tilde{\varepsilon}_{kl}) \quad \text{in } D. \tag{21}$$

The correction problem can be defined by taking a difference between the original inhomogeneous inclusion problem and the dislocation problem:

$$\hat{\sigma}_{ij} = C_{ijkl}(\varepsilon^0_{kl} + \hat{\varepsilon}_{kl}) + (C_{ijkl} - C^m_{ijkl})\tilde{\varepsilon}_{kl} - C^m_{ijkl}\varepsilon^{m,0}_{kl} \quad \text{in } D - \Omega, \tag{22}$$

$$\hat{\sigma}_{ij} = C^m_{ijkl}(\hat{\varepsilon}_{kl} + \varepsilon^m_{kl}) \quad \text{in } \Omega^m. \tag{23}$$

For the sake of simplicity, Eq. (22) can be rewritten as

$$\hat{\sigma}_{ij} = C_{ijkl}\hat{\varepsilon}_{kl} + \Sigma^D_{ij} \quad \text{in } D - \Omega, \tag{24}$$

where $\Sigma^D_{ij} = C_{ijkl}\varepsilon^0_{kl} + (C_{ijkl} - C^m_{ijkl})\tilde{\varepsilon}_{kl} - C^m_{ijkl}\varepsilon^{m,0}_{kl}$. Then, the correction problem defined by Eqs. (24) and (23) can be considered as a problem of an infinite body with an initial stress Σ^D_{ij} containing inhomogeneous inclusions with eigen strains. The boundary integral equations for the correction problem can be derived in a similar way to that used for deriving Eqs. (16) and (18):

$$\begin{aligned} c_{ij}(P)\hat{u}_j(P) = {} & \int_\Gamma U_{ij}(P,Q)\hat{t}_j(Q)\,\mathrm{d}\Gamma - \int_\Gamma T_{ij}(P,Q)\hat{u}_j(Q)\,\mathrm{d}\Gamma \quad \text{for } D - \Omega \\ & - \int_{D-\Omega} \Sigma^D_{jk}(q)U_{ij,k}(P,q)\,\mathrm{d}\Omega, \end{aligned} \tag{25}$$

$$\begin{aligned} c_{ij}(P)\hat{u}^m_j(P) = {} & \int_{\Gamma^m} U^m_{ij}(P,Q)\hat{t}^m_j(Q)\,\mathrm{d}\Gamma - \int_{\Gamma^m} T^m_{ij}(P,Q)\hat{u}^m_j(Q)\,\mathrm{d}\Gamma \quad \text{for } \Omega^m \\ & - \int_{\Omega^m} C^m_{jkln}\varepsilon^m_{ln}(q)U^m_{ij,k}(P,q)\,\mathrm{d}\Omega. \end{aligned} \tag{26}$$

Assuming that the eigen strain ε^m_{ij} is uniform in the mth inhomogeneous inclusion, Eq. (26) can be rewritten as

$$\begin{aligned} c_{ij}(P)\hat{u}^m_j(P) = {} & \int_{\Gamma^m} U^m_{ij}(P,Q)(\hat{t}^m_j(Q) + C_{jkln}\varepsilon^m_{ln}(Q)n_k(Q))\,\mathrm{d}\Gamma \\ & - \int_{\Gamma^m} T^m_{ij}(P,Q)\hat{u}^m_j(Q)\,\mathrm{d}\Gamma \quad \text{for } \Omega^m \\ = {} & \int_{\Gamma^m} U^m_{ij}(P,Q)\tilde{t}'^m_j(Q)\,\mathrm{d}\Gamma - \int_{\Gamma^m} T^m_{ij}(P,Q)\hat{u}^m_j(Q)\,\mathrm{d}\Gamma, \end{aligned} \tag{27}$$

where $\tilde{t}'^m_j$ is the actual traction on the interface between the infinite body and the mth inhomogeneous inclusion, which is defined by $\tilde{t}^m_j + C^m_{jkln}\varepsilon^m_{ln}$. To solve the boundary integral equations (25) and (27) by the multi-zone BEM, the infinite body with holes must be discretized by volume elements while the inhomogeneous inclusions can be modeled with only boundary elements. Then the equations cannot be solved by the BEM, because the discretization of the infinite body is definitely impossible. In order to calculate a stress at a point inside of the mth inhomogeneous inclusion, we must obtain only all the displacements $\hat{u}^m_j$ and the tractions $\tilde{t}'^m_j$ on the interface. An alternative equation to calculate the displacements $\hat{u}^m_j$ can be derived from the definition of the dislocation problem and the correction problem:

$$\hat{u}^m_j = u_j - \tilde{u}_j, \tag{28}$$

where u_j is the actual displacement. $\tilde{u}_j$ is the displacement produced by dislocation loops, which can be calculated by the fast sum method for displacements. The actual displacement on the interface can be obtained by solving Eqs. (16) and (18) by the multi-zone BEM. Therefore the displacement boundary condition to the mth inhomogeneous inclusion can be entirely determined by the above equation. Then the remaining unknown variable is only the traction on the interface, which can be calculated with Eq. (27) with the displacement boundary condition given by Eq. (28) without any coupling with the equation for the infinite body. Thus, in order to calculate the displacements and tractions on the interface, we need only the discretization of the boundary of the inhomogeneous inclusion, and do not need to discretize the infinite body with volume elements. Once all the displacements $\hat{u}^m_j$ and the tractions $\tilde{t}'^m_j$ are obtained by solving Eq. (27) with the displacement boundary condition defined by Eq. (28), the stress at a point inside of the mth

inhomogeneous inclusion can be calculated by

$$\hat{\sigma}_{ij}(p) = \int_{\Gamma^m} D^m_{ijk}(p,Q) t'^m_k \, d\Gamma - \int_{\Gamma^m} S^m_{ijk}(p,Q) u'^m_k \, d\Gamma, \tag{29}$$

where $D^m_{ijk}(p,Q)$ and $S^m_{ijk}(p,Q)$ are the kernel functions calculated by Eq. (20) with $U^m_{ij,k}(p,Q)$ and $T^m_{ij,k}(p,Q)$, respectively.

It is worth noting that there is a singularity in the image stress calculated by the boundary element method when the calculation point is close to the boundary. Also the stress of the dislocation involves a strong singularity within a range of the dislocation core. In this work, these singularities are simply removed by introducing a cut-off radius $r_c = 2b$, which is typically used as a radius for the dislocation core. The stresses within the cut-off distance are kept constant.

In this paper, the methodology of PDD and the boundary integral equations for precipitate problems are mainly for the isotropic materials. However, the effects of elastic anisotropy on the dislocation behavior and macroscopic plastic deformation are also of interest. Han et al. (2003) extended the PDD method to the anisotropic materials, and examined the accuracy and convergence of the method. Vogel and Rizzo (1973) proposed kernel functions for an anisotropic elastic body, which can be used in the boundary integral equations instead of the isotropic kernel functions. Applying these to the PDD and boundary integrals equations, the proposed method can also be easily and directly extended to the anisotropic materials.

4. Numerical accuracy and convergence

The accuracy of the present PDD and BEM procedure (PDD-BEM, for short) for inhomogeneous inclusion problems with dislocations is examined with an available analytical solution for the interaction between a screw dislocation and a spherical precipitate in an infinite body, given by Gavazza and Barnett (1974). This should establish the numerical accuracy of the procedure, and reveal control features needed for a required level of accuracy. We will also examine the range of applicability of elastic theory used here by comparing the results with atomistic simulations based on interatomic interactions, and performed with the method of molecular dynamics (MD). There are several studies using the MD technique for the interaction between an edge dislocation and a precipitate (Osetsky et al., 2003; Kohler et al., 2005). In this paper, we focus on the interaction between an edge dislocation and a copper precipitate in an iron matrix, and compare the results of MD with those of the present PDD-BEM approach.

4.1. Comparison with analytical solutions

Gavazza and Barnett developed an analytical solution for the image stress from an interface between a spherical precipitate in an infinite body in the presence of an infinitely long straight screw dislocation, given by

$$\begin{aligned}
\tau_{yz}(t,0,z) = & \sum_{n=1}^{\infty} \left\{ -a^{n+1}(2\mu_1\alpha_n + \mu_1\beta_n) + 6\mu_1 K_n \Omega_n \frac{2n+1}{2n+5} \right\} \frac{1}{r^{n+2}} P^{n-1}_{n+1} \\
& + \sum_{n=1}^{\infty} \left\{ -\frac{1}{2}\mu_1 a^{n+1}\beta_n + \mu_1 K_n \Omega_n \frac{2n+3}{2n+5} \right\} \frac{1}{r^{n+2}} P^{n+1}_{n+1} \\
& + \sum_{n=1}^{\infty} \left\{ 2\mu_1 \left(\frac{a^2}{r^2} - 1 \right) K_n \Omega_n + \mu_1 K_n \Omega n \frac{2}{2n+5} \right\} \frac{1}{r^{n+2}} P^{n+1}_{n+3} \\
& + \sum_{n=1}^{\infty} \left\{ 24\mu_1 \left(\frac{a^2}{r^2} - 1 \right) K_n \Omega_n + \mu_1 K_n \Omega_n \frac{24}{2n+5} \right\} \frac{1}{r^{n+2}} P^{n-1}_{n+3},
\end{aligned} \tag{30}$$

where a is the radius of the spherical precipitate, μ_1 is the elastic shear modulus of the infinite body, P^m_n is the Legendre function of $\cos\phi$, and

$$K_n = -\frac{\lambda_1 + \mu_1}{2\{(n+2)\lambda_1 + (3n+5)\mu_1\}},$$

$$\Omega_n = \frac{2\eta_n(\mu_1-\mu_2)a^{2n+1}/t^n}{\mu_1\{(n+2)+E_n^I(2n+1)(n+1)\}+\mu_2(2n)},$$

$$\alpha_n = \frac{(\mu_1-\mu_2)\eta_n}{\mu_1(n+2)+\mu_2(n-1)}\frac{\mu_1\{(n+2)-E_n^I(2n+1)(n-1)\}}{\mu_1\{(n+2)+E_n^I(2n+1)(n+1)\}+\mu_2(2n)}\left(\frac{a}{t}\right)^n,$$

$$\beta_n = \frac{(\mu_2-\mu_1)\eta_n}{\mu_1(n+2)+\mu_2(n-1)}\frac{\mu_1\{(n+2)+E_n^I(2n+1)(n-1)\}+2\mu_2(n-1)}{\mu_1\{(n+2)+E_n^I(2n+1)(n+1)\}+\mu_2(2n)}\left(\frac{a}{t}\right)^n,$$

$$\eta_n = \left(\frac{b}{4\pi}\right)\frac{(-1)^n 2^n(n-1)!}{(2n-1)!},$$

$$E_n^I = \frac{(n-1)\lambda_1-(n+4)\mu_1}{(2n+1)(n+2)\lambda_1+(3n+5)\mu_1}, \tag{31}$$

where λ_1 is Lame's constant of the infinite body, and μ_2 is the elastic shear modulus of the precipitate.

In the PDD-BEM simulation of the above problem, the simulation volume is taken as the infinite body with an elastic shear modulus $\mu_1 = 81.8\,\text{GPa}$, and contains a spherical precipitate with a diameter $d = 2.5\,\text{nm}$ and an elastic shear modulus $\mu_2 = 54.6\,\text{GPa}$. We place an infinitely long straight screw dislocation with a Burgers vector $b = 0.248\,\text{nm}$ into the simulation volume. The stress field of the dislocation is analytically calculated with a stress solution for the screw dislocation. The image stresses from the interface between the infinite body and the precipitate are calculated at the center of the screw dislocation within a range from $0.5d + 2b$ to $2.5d$ away from the center of the precipitate by putting the screw dislocation at several positions in this range.

To illustrate the convergence and accuracy of the accuracy of image stress calculations, we used four boundary and volume element mesh sizes, resulting in different spatial resolutions, as shown in Fig. 2. Throughout the present work, 8-noded and 20-noded isoparametric elements are used for the boundary and volume elements of the precipitates, respectively. As an expression of the resolution of the boundary element mesh, we use a non-dimensional parameter γ, defined as the ratio of the average boundary element to total interface areas.

Fig. 3 shows the dependence of the image shear stress on the relative distance from the precipitate center. The present PDD-BEM results are displayed together with Gavazza and Barnett's analytical solution given by Eq. (30). In the figure, the image stress decreases sharply and becomes negative within the range of $1.5d$. The errors of the calculated image stresses in comparison with the analytical solution are plotted in Fig. 4. In the figure, the mesh with $\gamma = 0.167$ gives unacceptable errors of more than 25%. It is especially noted that the error becomes large near the interface between the infinite body and the precipitate. This might be due to the singularity in the image stress calculation. The accuracy of the image stress rapidly improves as the resolution of the mesh is increased. In the case of the mesh with $\gamma = 0.0104$, the maximum error of the image stress is almost 0.6%, which can be acceptable as high accuracy for the purposes of DD simulations. Therefore, the

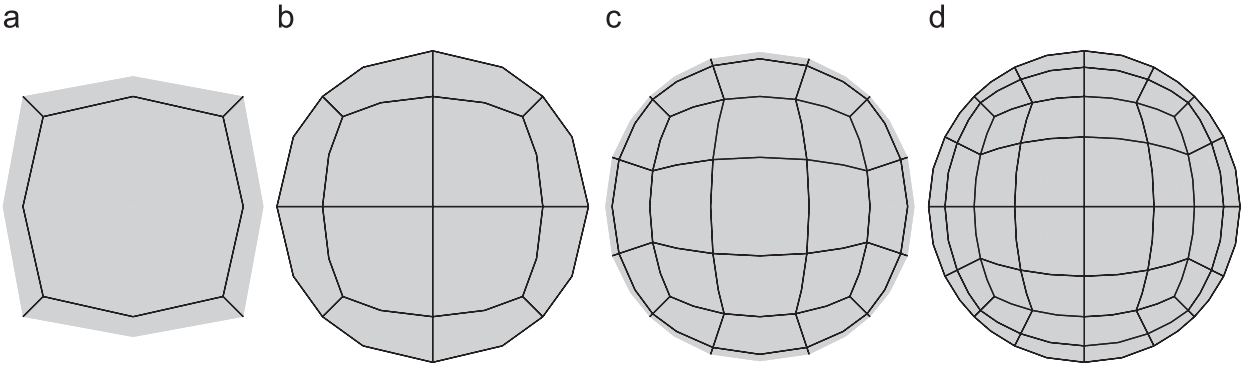

Fig. 2. Boundary element meshes for a spherical precipitate: (a) $\gamma = 0.167$; (b) 0.0417; (c) 0.0185; and (d) 0.0104.

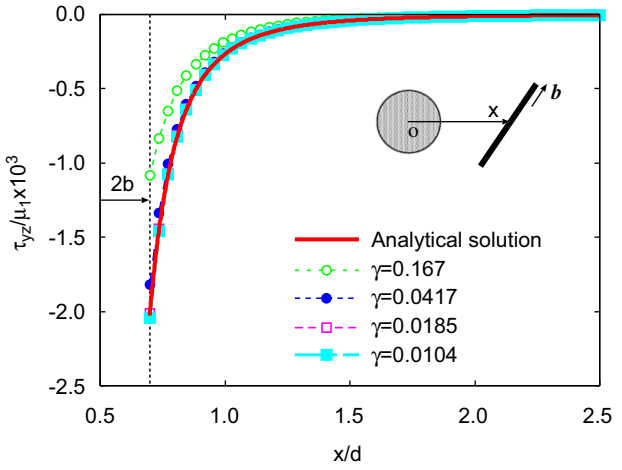

Fig. 3. Image stresses generated by an interface between a precipitate and an elastic body in the presence of an infinitely long straight screw dislocation. The image stresses are calculated by the present PDD-BEM method, and are at the closest point on the screw dislocation to the precipitate. The analytical solution given by Gavazza and Barnett is also plotted with a solid line. As shown in the figure, x is the closest distance between the screw dislocation and the center of the precipitate.

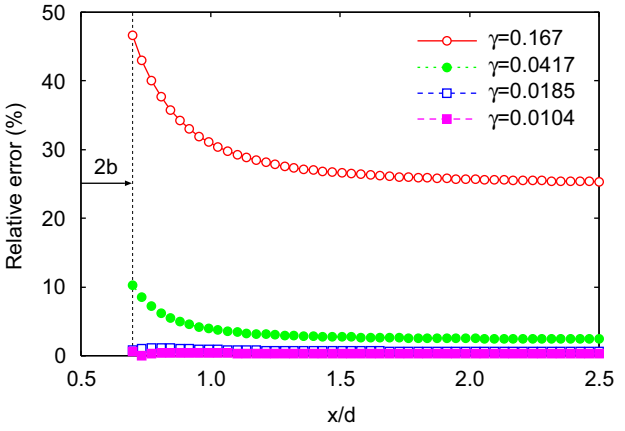

Fig. 4. Relative error of image stresses calculated by the present PDD-BEM method as compared to the analytical solution given by Gavazza and Barnett.

results suggest that the PDD-BEM method has excellent convergence rates and accuracy with boundary mesh refinement.

4.2. Comparison with molecular dynamics

One of the key phenomena that determine the degree of embrittlement of pressure vessel steels is the interaction between dislocations in an iron matrix with small copper and copper–iron precipitates in steels. Several MD simulations have been carried out to determine the atomistic origins of this interaction, for example the MD simulations of the interaction between an edge dislocation and a spherical copper precipitate (Osetsky et al., 2003). For iron–copper precipitates, on the other hand, Kohler et al. (2005) performed MD simulations of the interaction using an embedded atom method (EAM) interatomic potential for iron–copper binary alloys. In these studies, the size of the simulation volume is $19.7 \times 19.7 \times 9.73$ nm, and the x, y and z axes are along $[1\,1\,\bar{2}]$, $[1\,1\,1]$ and $[1\,\bar{1}\,0]$ directions, respectively. A spherical copper precipitate with a diameter d_{Cu} and an edge dislocation with $[1\,1\,1]$ Burgers vector on $(1\,\bar{1}\,0)$ slip plane are placed in the volume. The center

of the copper precipitate is on the slip plane of the dislocation. Periodic boundary conditions are applied along $[1\,1\,\bar{2}]$ direction, which implies that the edge dislocation is infinitely long, and that the precipitate is one of a periodic array in the $[1\,1\,\bar{2}]$ direction. The CSS for the edge dislocation to break away from the copper precipitate is evaluated by applying and gradually increasing the external shear stress.

In the PDD-BEM simulation of the interaction, the same simulation volume is used, with boundary and volume elements for the copper precipitate and parametric segments for the edge dislocation. Kohler et al. calculated the elastic constants of the iron matrix and the copper precipitate using the interatomic potential. Their calculated elastic shear modulus for the iron matrix and copper precipitate are $\mu_1 = 69.76\,\text{GPa}$ and $\mu_2 = 21.842\,\text{GPa}$, respectively. Although the experimental values of the shear moduli are higher, we used the same elastic constants of Kohler et al. (2005) in the present PDD-BEM simulations. This allows direct comparison between the elasticity results (present model) and the results of MD simulations, which are based on interatomic potentials. The CSS is evaluated by gradually increasing the external shear stress by 5 MPa each 1000 time steps. In order to examine the convergence of the accuracy of the PDD-BEM method, we used different boundary and volume element mesh densities resulting in successively higher resolution, while the length of each parametric segment is set to be 1 nm in all simulations.

Before showing the results of the accuracy and convergence of the PDD-BEM method, we evaluated the computation time. Since the precipitate shape is not changed in the simulation, once the stiffness matrix of the boundary integral equations is calculated and decomposed into lower and upper (LU) matrices, it is not necessary to do the same thing at every time step. The LU matrices of the stiffness matrix calculated at the first time step are stored, and can be repeatedly used at every time step to compute quickly the displacements and tractions on the interface between the precipitate and the matrix. Therefore, in the evaluation, we checked two kinds of computation time: (1) the computation time to integrate the boundary integral equation and to decompose it into LU matrices and (2) the computation time for each time step. Fig. 5 shows the computation time. Regarding to the time for the calculation and decomposition of the stiffness matrix, it is rapidly increased as the number of nodes for the boundary elements is increased. Generally, the amount of the computation for the calculation of the stiffness matrix is proportional to the square of the number of nodes, and, for the decomposition, it is proportional to cube of the number of nodes. Thus the trend of the computation time is reasonable. On the other hand, as for the time for each time step, the relationship between the computation time and the number of nodes is approximately linear. If the decomposed LU matrices are not stored, we need almost the same computation time as that for the calculation and decomposition of the stiffness matrix. Therefore, the storage of the decomposed LU matrices greatly improves the efficiency and speed of the PDD-BEM simulations.

Fig. 6 shows the dislocation configurations during the interaction with a 3 nm diameter copper precipitate. In the figure, the dislocation is first attracted by the copper precipitate. The dislocation then moves spontaneously to the middle of the copper precipitate to achieve equilibrium in the precipitate interior.

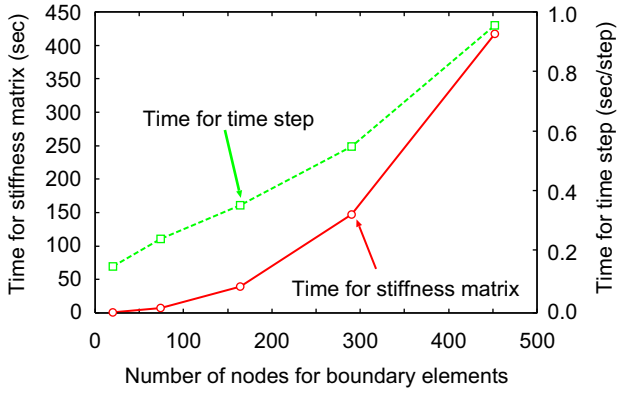

Fig. 5. Computation time for (1) calculating and decomposing the stiffness matrix of the boundary integral equations and (2) each time step. In the evaluation of the computation time, the boundary and volume element meshes for the simulations of interaction between a dislocation and a copper precipitate are used.

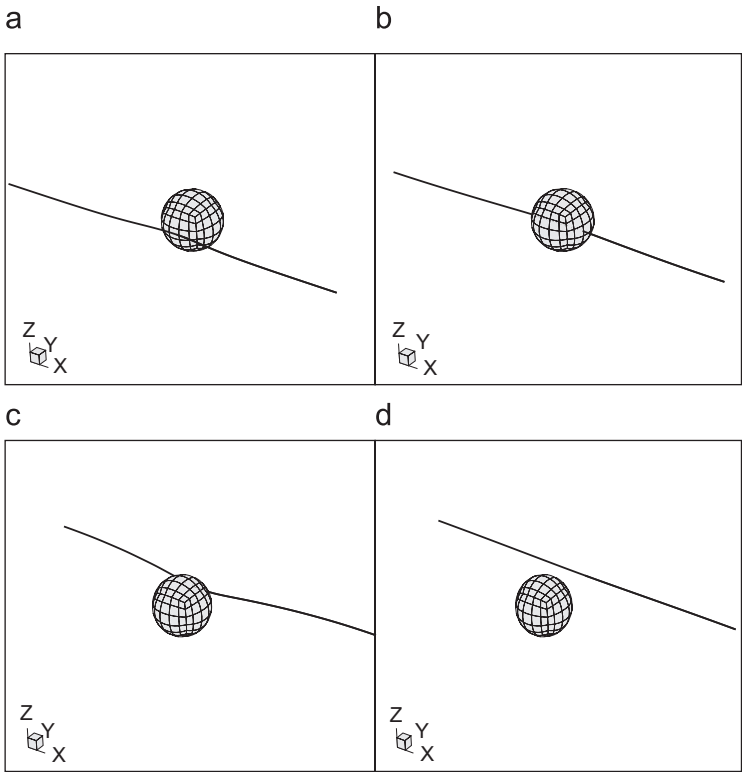

Fig. 6. Configurations of the edge dislocation interacting with the copper precipitate with $d_{Cu} = 3.0$ nm. (a) and (b) are the configurations during the process to reach an equilibrium configuration from the initial straight dislocation. (c) is the configuration of the most bent dislocation configuration due to interaction with the precipitate. (d) is after the interaction.

A higher force is required to pull the dislocation out of the precipitate, and thus the precipitate temporarily pins the dislocation till a higher force is applied. Finally the dislocation cuts through the copper precipitate when the external shear stress is sufficiently increased resulting in a break-away configuration (Fig. 6-d).

Fig. 7 shows the dependence of the CSS on precipitate diameter, calculated by the PDD-BEM method and compared to the results of MD simulations (Kohler et al., 2005). In the figure, the CSS calculated with a coarse mesh ($\gamma = 0.167$) displays a large deviation from MD simulation results. However, the CSS converges gradually to MD results as the mesh resolution is increased (smaller γ values). Note that the results for $\gamma = 0.0104$ and 0.00667 are almost the same indicating convergence, and that the results are in reasonable agreement with MD simulations. The difference between the PDD-BEM and MD simulation results at large diameters is attributed to using a constant cut-off radius $2b$ to avoid the stress singularity. This difference can be corrected for by adjusting the cut-off distance as a function of precipitate size, which we did not attempt here for clarity of comparison.

Kohler et al. (2005) also performed MD simulations for the interaction between an edge dislocation and an iron–copper complex with a diameter $d_{Cu} = 2.5$ nm in an iron matrix. They used the same simulation volume, and calculated the CSS of the iron–copper complex with various copper concentrations. Here, we compare their MD results with our PDD-BEM calculations. In the PDD-BEM simulations, the same simulation volume is used. The elastic constants of the iron–copper complex is determined by two types of averaging procedures, namely the Voigt and Reuss approximations. The calculated elastic constants with these rules are listed in Table 1, where it is noted that the Reuss approximation gives smaller elastic constants compared to the Voigt approximation. Fig. 8 displays the dependence of the CSS on the atomic fraction of Fe in the copper precipitate. The PDD-BEM simulation results with the elastic constants calculated by the Voigt approximation show an approximate linear dependence on the Fe atomic fraction, which is clearly different from the results of the MD simulations. On the other hand, PDD-BEM simulation results with the elastic

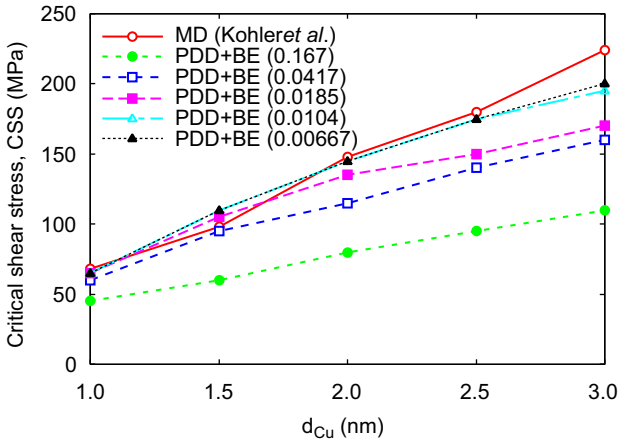

Fig. 7. Dependence of the critical shear stress (CSS) for an edge dislocation in Fe cutting through a copper precipitate on its diameter. Results of PDD-BEM calculations are compared to the MD computer simulations by Kohler et al. The numbers in brackets are the γ values, indicative of the boundary element mesh resolution.

Table 1
Elastic shear modulus (GPa) for iron–copper complexes calculated by two different rules of mixture: the Voigt and Ruess approximations

Rule of mixture	25%	50%	75%
Voigt	33.8	45.8	57.8
Ruess	26.4	33.3	45.1

The percentage in the table is the concentration of iron in the complex.

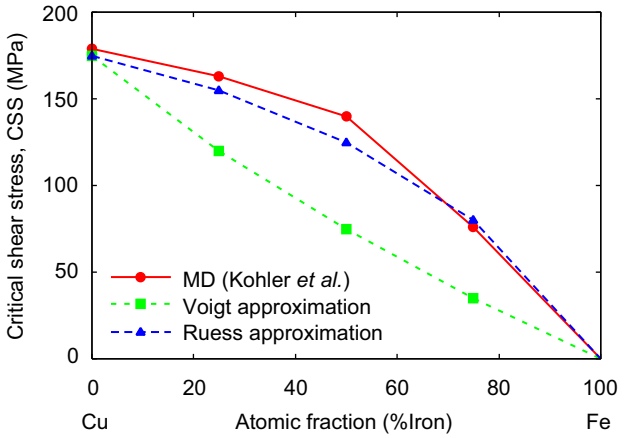

Fig. 8. Critical shear stresses of iron–copper complexes of a fixed diameter (2.5 nm) calculated by the PDD-BEM method. The results of MD simulations obtained by Kohler et al. are also plotted in the figure. The elastic constants of the iron–copper complexes used in the PDD-BEM simulations are calculated by two different rules of mixture: the Voigt and Ruess approximations.

constants calculated by the Reuss approximation are in good agreement with MD simulations, indicating that the result of the PDD-BEM simulation is very consistent with MD simulations, when the Reuss approximation is used. This greatly simplify the process of alloy optimization with the present method, as compared to the limitations of MD simulations and the need to develop interatomic potentials for various Fe–Cu mixtures within the precipitate.

5. Applications

5.1. Dislocation interaction with sheared precipitates

When the shear modulus of precipitates is below the Orowan limit (see next section), they can be sheared by the passage of dislocations through them. Every time a dislocation shears, its resistance to dislocation motion is reduced. If the precipitate is sheared a number of times, and the overall resistance of the two sheared pieces becomes sufficiently low, many dislocations can slip through the sheared region in an avalanche fashion, and a zone of localized plastic deformation is formed in the matrix. This mechanism can result in plastic flow localization and the formation of cleared dislocation channels in precipitation hardened materials. In this section, we evaluate the CSS of precipitates with a diameter of 2.5 nm and an elastic shear modulus $\mu_p = 54.6$ GPa cut by dislocations in an Fe matrix. Every time the precipitate is completely sheared, the two halves are shifted relative to one another by the magnitude of the Burgers vector and two new surfaces on the slip plane of the dislocation are formed. Although the formation and progress of the slip step during the dislocation cuttings should give an effect on the CSS, it is neglected here as a consequence of the traditional infinitesimal strain approximation. To simulate the process of dislocation interaction with shared precipitates, we conducted a series of simulations where the precipitate is initially shared by different degrees. The initial state of the shared precipitate is assumed to be stress-free, and the dislocation is assumed to approach the precipitate, which is already in a shared state that may have been created by the passage of previous dislocations. In other words, we performed multiple infinitesimal strain calculations starting from a stress-free initial configuration, and hence neglected the effect of precipitate deformation history. In the following series of simulations, we use a volume of $19.7 \times 19.7 \times 9.73$ nm, with the x, y and z axes along the $[1\,1\,\bar{2}]$, $[1\,1\,1]$ and $[1\,\bar{1}\,0]$ directions, respectively. A straight edge dislocation with $[1\,1\,1]$ Burgers vector on the $(1\,\bar{1}\,0)$ slip plane that cuts through the middle of a spherical precipitate are placed in the simulation volume. Periodic boundary conditions are applied along the $[1\,1\,\bar{2}]$ direction, which correspond to a periodic 1D array of precipitates. The elastic constants of the iron matrix is taken as $\mu_m = 81.8$ GPa. Fig. 9 shows an example of a boundary element mesh of the slipped precipitate. As shown in the figure, the boundary elements for the newly created surfaces of the copper precipitate are first generated in a simple manner, and are then improved using a Laplacian smoothing technique (Field, 1988). Moreover, multiple nodes are located along the edge lines of the newly created surface of the precipitate to represent the geometrical discontinuity. A multiple collocation approach (MCA) is utilized only for multiple nodes to solve the problem accurately (Dominguez et al., 2000). In the simulations, the external shear stress is increased by 1 MPa each 1000 time steps to determine the CSS.

Fig. 10 shows the dislocation configuration during the interaction with a 2.5 nm diameter precipitate that has been completely sheared by the passage of 10 previous dislocations (i.e. the two hemispheres are shifted 10 b with respect to one another). As the dislocation glides along the surfaces of the two precipitate halves, it is partially locked at the edges, thus forming bow-out pinned configurations. The dislocation bow-out is slightly extended by the external shear stress and the pinning effect of the precipitate. Finally, the dislocation breaks

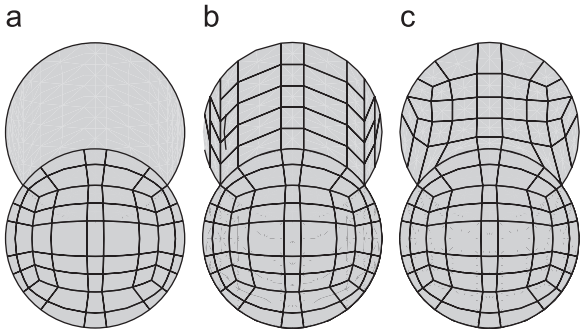

Fig. 9. Boundary element mesh generation for newly created surfaces by dislocation cuttings. (a) Slipped precipitate without any boundary element mesh for the newly created surface, (b) manually generated boundary elements for the newly created surface, and (c) improved boundary elements using a Laplacian smoothing technique.

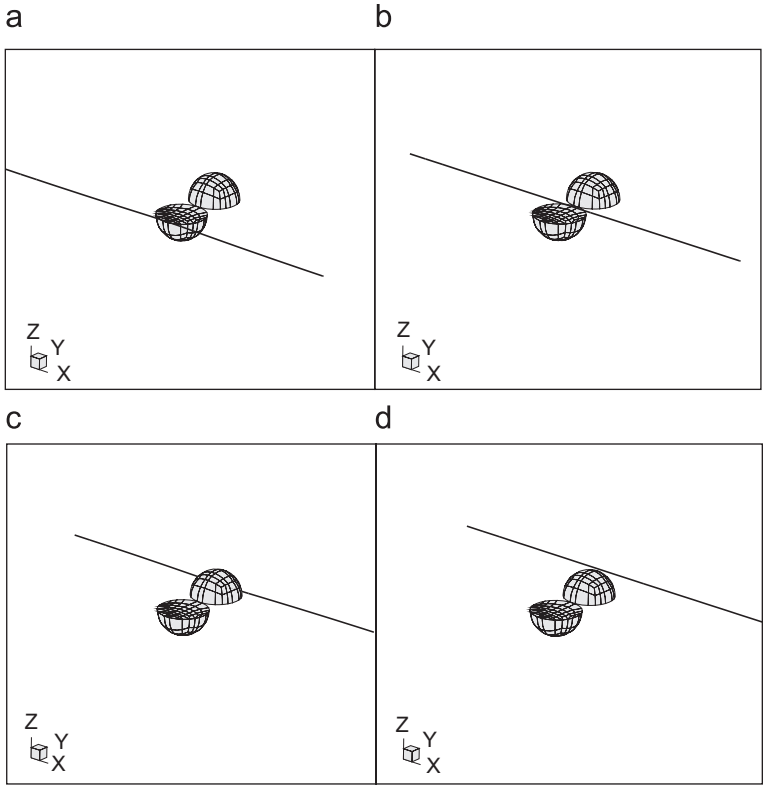

Fig. 10. Configurations of the edge dislocation interacting with the slipped copper precipitate. The precipitate halves are displaced by 10 b. (a) and (b) are the configurations during the process of reaching equilibrium from the initial straight dislocation configuration. (c) is the most bent dislocation configuration by the precipitate. (d) after the interaction.

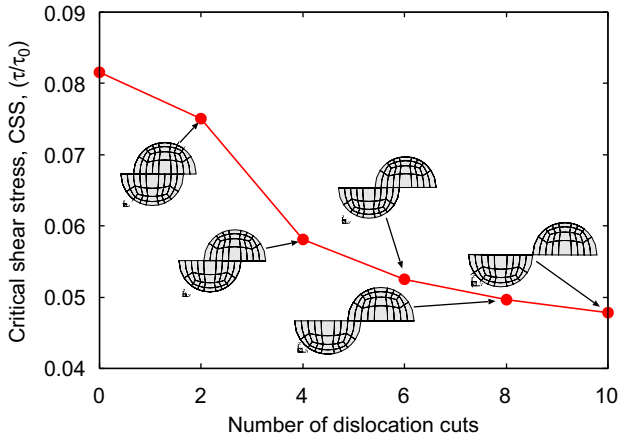

Fig. 11. The dependence of the relative critical shear stresses of the slipped precipitates on the number of dislocation "cuttings". The critical shear stress is normalized by $\tau_0 = \mu_m b/L$.

away from the precipitate when the external shear stress is sufficiently increased. Fig. 11 shows the calculated "relative" CSS of slipped precipitates as a function of the number of previous dislocation passages or "cuttings" through the precipitate. Note that the CSS is normalized by $\tau_0 = \mu_m b/L$, where L is the spacing between the precipitates. It is shown that the CSS rapidly decreases each time the precipitate is cut by

a dislocation. As the number of the dislocation cuttings is increased, the CSS decreases further, but gradually converges to a constant value. We also performed a PDD-BEM simulation for the interaction between an edge dislocation and half of a precipitate, which corresponds to a precipitate slipped an infinite number of dislocation cuttings. The calculated relative CSS was found to be $0.0431\tau_0$, which is almost half of the CSS of the spherical precipitate. The present PDD-BEM simulations reveal that the resistance of precipitates to dislocation motion is rapidly weakened by previous dislocation cuttings, and may decrease to about half of the CSS of an uncut spherical precipitate.

5.2. The influence of precipitate geometric and elastic parameters on strength

Precipitation strengthening is derived from a number of factors, such as precipitate geometry, spatial arrangement, and the relative magnitude of the elastic modulus compared to the host matrix. One of the important aspects here is the effect of the elastic modulus mismatch between the precipitate and the host matrix. If the shear modulus of the precipitate is smaller than that of the matrix, dislocations can easily cut through the precipitate. Even if the precipitate shear modulus is somewhat larger than that of the matrix, the dislocation can still cut through the precipitate and reconfigure to its original form before the interaction. However, precipitates with much larger elastic modulus compared to the matrix can present impenetrable obstacles to dislocation motion. In this case, dislocations must completely encircle the precipitate and leave a small loop surrounding the precipitate before they reconfigure and break-away from the precipitate. This interaction limit is known as the Orowan mechanism.

In this section, utilizing PDD-BEM simulations, we investigate the influence of a number of important geometric and elastic parameters on the CSS, and hence on the strengthening effect of precipitates. These are: (1) the precipitate diameter, (2) the spacing between precipitates, and (3) the ratio of the precipitate-to-matrix shear modulus. The simulation volume is $50 \times 50 \times 50$ nm, with the x, y and z axes taken along the $[1\,1\,\bar{2}]$, $[1\,1\,1]$ and $[1\,\bar{1}\,0]$ directions, respectively. A spherical precipitate with a diameter of 5 nm is placed in the middle of the simulation volume. A straight edge dislocation with $[1\,1\,1]$ Burgers vector on the $(1\,\bar{1}\,0)$ slip plane is also introduced, and is initially placed 10 nm away from the precipitate. Periodic boundary conditions are applied along the $[1\,1\,\bar{2}]$ direction to simulate the interaction of a one-dimensional precipitate array with the dislocation. The elastic shear modulus of the matrix material μ_m is taken as 81.8 GPa, and of the precipitate shear modulus, μ_p, is changed in the range from $0.01 \leqslant \mu_m/\mu_p \leqslant 5$ in order to investigate the effect of the elastic modulus mismatch between the precipitate and the matrix on the CSS.

To investigate the influence of the precipitate diameter and modulus on the strength, a set of simulations were performed for a range of precipitate-to-matrix shear modulus ratios, and for initial precipitate diameters of 5, 7.5, and 10 nm. The results of the PDD-BEM simulations are shown in Fig. 12, where the CSS is normalized by the reference shear stress $\tau_0 = \mu_m b/L$. It is shown that larger precipitates have a stronger strengthening effect, and that the CSS is dependent also on the relative elastic modulus mismatch. Softer precipitates ($\mu_p/\mu_m \leqslant 1$) still result in strengthening ($\tau/\tau_0 > 0$), and in the limit of very soft precipitates (e.g. voids), the strengthening effect saturates to $\tau/\tau_0 \approx 0.3 - 0.4$. On the other hand, harder precipitates are still shearable up to μ_p/μ_m ratios on the order of 3–4, where the Orowan looping mechanism sets in, as shown in the figure with hollow symbols. It is also noted that the strength sensitivity to the μ_p/μ_m ratio in the Orowan regime is considerably smaller than in the shearable precipitate regime.

The transition from the shearable precipitate to the Orowan regime depends on the precipitate size, as shown in the figure. The self-force on the dislocation surrounding the precipitate mainly depends on the diameter of the precipitate, and is large when the diameter of the precipitate is small. For small precipitates, the dislocation prefers to cut through them as a result of the strong self-force on the dislocation. Therefore, the precipitate with a small diameter must have a large elastic shear modulus to stop the dislocation from cutting it, and hence the onset of the Orowan mechanism must take place at larger μ_p/μ_m values for a precipitate with a smaller diameter.

Next, we investigate the effect of the inter-precipitate spacing on the strengthening effect by changing the length of the simulation volume in the $[1\,1\,\bar{2}]$ direction to 50, 75, and 100 nm. The results of the PDD-BEM simulations are shown in Fig. 13, where the CSS is normalized by the reference shear stress with different values of L. It is clear from the figure that the normalized shear stress is insensitive to the inter-precipitate

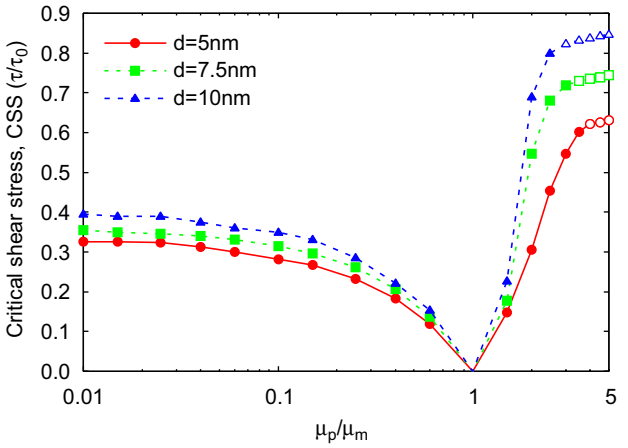

Fig. 12. Dependence of the CSS on the precipitate-to-matrix shear modulus ratio. The effect of the precipitate diameter on the strength is shown, where the solid symbols are for dislocations cutting through precipitates while the hollow symbols are for dislocations looping around the precipitate by the Orowan mechanism.

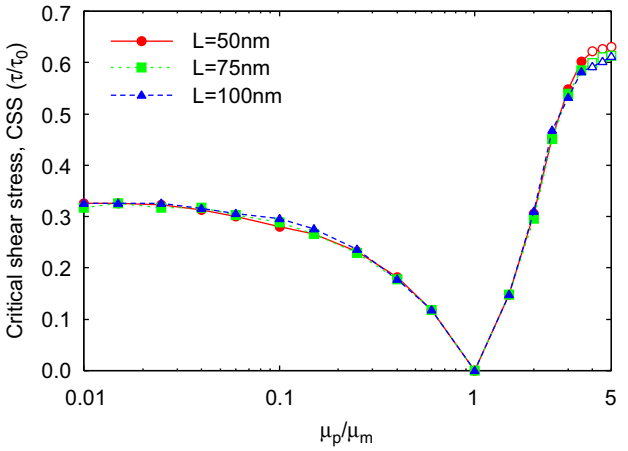

Fig. 13. Critical shear stresses of precipitates with different inter-precipitate spacings and elastic constants calculated by the PDD-BEM method. The solid symbols indicate that the dislocation cuts through the precipitate, while the hollow symbols are associated with the Orowan mechanism.

spacing over a wide range of μ_p/μ_m ratios. This is indicative of the direct inverse proportionality between the CSS and L, as predicted by the Orowan formula. Small deviations from the inverse proportionality can be seen for very large μ_p/μ_m ratios, indicating a slight dependence on the precipitate size as well.

6. Discussion and conclusions

Nembach studied the interaction between an infinitely long straight dislocation and a precipitate, and developed an equation to calculate the CSS, accounting for the effect of the difference in the elastic shear modulus between the precipitate and the matrix (Nembach, 1983). The work is based on Friedel's approximation for the CSS τ_{cF} (Friedel, 1964), given by

$$\tau_{cF} = C_F \frac{F_0^{3/2} f^{1/2}}{r_p b (2\pi S)^{1/2}}, \tag{32}$$

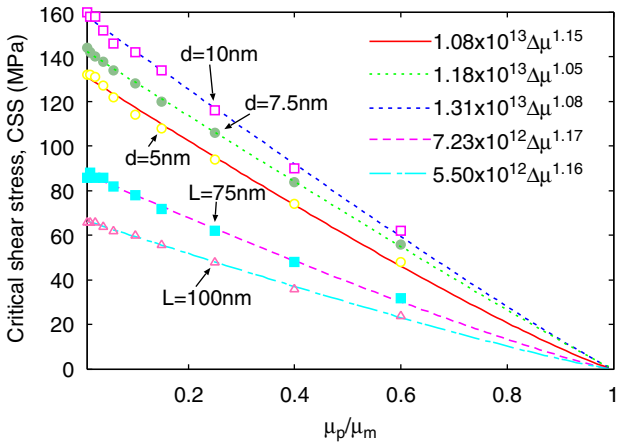

Fig. 14. Curve fits to PDD-BEM simulation results with different values of the precipitate radius and inter-precipitate spacing. The results of the PDD-BEM simulations are shown with symbols, while the curve fits are the lines.

where C_F is the numerical constant, S is the dislocation line tension, and r_p and f are the radius and volume fraction of the precipitates, respectively. F_0 is the maximum interaction force between the dislocation and the precipitate, and is proportional to the difference in the elastic shear modulus between the precipitate and matrix, $\Delta\mu$. Nembach fitted the calculated maximum interaction force to the following equation:

$$F_0 = \alpha_1 \Delta\mu b^2 \left(\frac{r_p}{b}\right)^{\beta_1}, \tag{33}$$

where α_1 and β_1 are adjustable parameters. Substituting Eq. (33) into Eq. (32), the following expression for the CSS is obtained (Nembach, 1983):

$$\tau_{cF} = C_F \frac{(\Delta\mu b^2)^{3/2} \alpha_1^{3/2} r_p^{(3\beta_1/2-1)} f^{1/2}}{b^{(3\beta_1/2+1)} (2\pi S)^{1/2}}. \tag{34}$$

From Eq. (34), the CSS of is proportional to $\Delta\mu^{1.5}$. Based on this work, we fitted the results of PDD-BEM simulations for the CSS to an equation of the form $\tau_{cF} = \alpha\Delta\mu^{\beta}$. The fitted curves for the CSS are plotted in Fig. 14. As shown in the figure, the exponents β are almost the same in all cases, with an average value of 1.12, which differs from the analytically estimated exponent of 1.5. This may be attributed to the fact that the Friedel approximation is for a system with randomly distributed precipitates. However, in our PDD-BEM simulations, the precipitates are situated as a regular 1-D array as a result of periodic boundary conditions, and have a constant inter-precipitate spacing. Therefore, instead of using Friedel's approximation for the present comparison, we use an equation for a system with the regular array of precipitates, given by

$$\tau_{cF} = \frac{F_0}{bL}. \tag{35}$$

Substituting Eq. (33) into Eq. (35), we have

$$\tau_{cF} = \frac{\Delta\mu b^2 \alpha_1 r_p^{\beta_1}}{b^{\beta_1+1} L}. \tag{36}$$

The equation shows that the CSS is proportional to the difference in the elastic shear moduli. Thus, based on Eq. (36), the exponent of 1.12, calculated from the PDD-BEM simulation results is in reasonable agreement with the analytically estimated exponent value of 1. The slight difference between the exponents should be attributed to the fact that the dislocation line is flexible in PDD-BEM simulations, while the dislocation line is straight in the analytical estimation.

The development of the present PDD-BEM method of computer simulations for precipitate–dislocation interactions has been shown to give accurate results in comparison with both analytical theory and MD simulations. The method can be a powerful tool for investigations of dislocation–precipitate interactions and

alloy design as compared to the MD technique, which is limited by both simulation volume size and the availability of a well-calibrated interatomic potential . However, the present PDD-BEM method takes into account only the elastic interaction between dislocations and precipitates, ignoring contributions form interaction forces within the dislocation core. Dislocation core effects may be dominant in small-size precipitates. To incorporate dislocation core effect in the framework of the PDD-BEM method, the Pierels–Nabarro (PN) model, which is a description of the dislocation core displacement based on the elasticity (Nabarro, 1947) can be used. With the PN model, the dislocation core displacement can be calculated by balancing the elastic interaction between infinitesimal displacements and the lattice restoring force that can be readily calculated from ab initio models. Using a reliable lattice restoring force, the PN model gives a more realistic displacement distribution within the dislocation core. Banejee et al. (2004) implemented the PN model into the PDD simulation framework, and represented the dislocation core displacement with an array of infinitesimal dislocations with distributed Burgers vectors. The lattice restoring force was calculated by taking the derivative of the γ surface energy, which can be computed by ab initio methods (Lu et al., 2000). Such a method can be utilized as a promising approach to incorporate the influence of the dislocation core on the CSS.

Before closing, we summarize here the salient results of the present work:

(1) A new computational method for the dynamics of the most general dislocation–precipitate interaction in 3-D has been successfully developed.
(2) The method, which is based on a natural hybridization of the parametric dislocation dynamics (PDD) and the boundary element method (BEM), PDD-BEM for short, is numerically accurate and convergent, and is in excellent agreement with MD computer simulation results.
(3) Calculations with the present PDD-BEM technique of the CSS for Cu–Fe complexes in an Fe matrix result in good agreement with MD simulations when the Reuss averaging scheme is used for the elastic constants.
(4) Sheared copper precipitates lose some of their resistance to dislocation motion after they are cut by leading dislocations in a pileup. Successive cutting of precipitates by the passage of a dislocation pileup reduces the resistance to about half its original value, when the number of dislocations in the pileup exceeds about 10.
(5) Precipitation strengthening can be achieved by precipitates that are either softer or harder than the host matrix. However, the largest gains in strengthening take place when the ratio of precipitate-to-matrix elastic modulus is not too large or too small. The most critical range for the effect of this ratio is between 0.1 and 4.
(6) The transition from the shearable precipitate regime to the Orowan looping regime occurs for precipitate-to-matrix elastic modulus ratios above approximately 3–4, with some dependence on the precipitate size.
(7) The CSS is shown to be inversely proportional to the inter-precipitate spacing over a very wide range of precipitate-to-matrix modulus ratios. Small deviations take place at high ratios in the Orowan regime.
(8) For a regular precipitate array of the same size, the relationship between the CSS and the difference in the shear modulus of the matrix and precipitate ($\Delta\mu$) is shown to be proportional to $\Delta\mu^{1.16}$.

Acknowledgments

This research is supported by the department of Energy, Office of Nuclear Energy, under the Nuclear Energy Research Initiative (NERI), grant number DE-FC07-06ID14748 at UCLA.

References

Banejee, S., Ghoniem, N.M., Kioussis, N., 2004. A computational method for determination of the core structure of arbitrary-shape 3D dislocation loops. In: Proceedings of MMM-2, pp. 23–25.

Devincre, B., Kubin, L.P., 1994. Simulations of forest interactions and strain hardening in fcc crystals. Modelling Simul. Mater. Sci. Eng. 2, 559–570.

Dominguez, J., Ariza, M.P., Gallego, A., 2000. Flux and traction boundary elements without hypersingular or strongly singular integrals. Int. J. Numer. Meth. Eng. 48, 111–135.

Eshelby, J.D., 1957. The determination of the elastic field of an ellipsoidal inclusion, and related problems. Proc. R. Soc. A 241 (1226), 376–396.
Field, D.A., 1988. Laplacian smoothing and Delaunay triangulations. Comm. Appl. Numer. Meth. 4, 709–712.
Fleischer, R.L., 1961. Solution hardening. Acta Metall. 9, 996–1000.
Fleischer, R.L., 1963. Substitutional solution hardening. Acta Metall. 11, 203–209.
Friedel, J., 1964. Dislocations. Pergamon Press, Oxford.
Gavazza, S.D., Barnett, D.M., 1974. The elastic interaction between a screw dislocation and a spherical inclusion. Int. J. Engng. Sci. 12, 1025–1043.
Ghoniem, N.M., 1999. Curved parametric segments for the stress field of 3-D dislocation loops. Trans. ASME J. Eng. Mater. Tech. 121 (2), 136.
Ghoniem, N.M., Sun, L.Z., 1999. Fast-sum method for the elastic field of three-dimensional dislocation ensembles. Phys. Rev. B 60 (1), 128–140.
Ghoniem, N.M., Tong, S.-H., Sun, L.Z., 2000. Parametric dislocation dynamics: a thermodynamics-based approach to investigations of mesoscopic plastic deformations. Phys. Rev. B 61, 913–927.
Gracie, R., Ventura, G., Belytschko, T., 2007. A new fast method for dislocations based on interior discontinuities. Int. J. Numer. Meth. Eng. 69, 423–441.
Han, X., Ghoniem, N.M., Wang, Z., 2003. Parametric dislocation dynamics of anisotropic crystals. Phil. Mag. 83 (31–34), 3705–3721.
Kohler, C., Kizler, P., Schmauder, S., 2005. Atomic simulation of precipitation hardening in α-iron: influence of precipitate shape and chemical composition. Modelling Simul. Mater. Sci. Eng. 13, 35–45.
Lu, G., Kioussis, N., Bulatov, V.V., Kaxiras, E., 2000. Generalized-stacking-fault energy surface and dislocation properties of aluminum. Phys. Rev. B 62 (5), 3099–3107.
Mura, T., 1982. Micromechanics of Defects in Solids. Martinus Nijhoff, Dordrecht.
Nabarro, F.R.N., 1947. Dislocations in a simple cubic lattice. Proc. Phys. Soc. 59, 256–272.
Nembach, E., 1983. Precipitation hardening caused by a difference in shear modulus between particle and matrix. Phys. Stat. Sol. (A) 78, 571–581.
Osetsky, Y.N., Bacon, D.J., Mohles, V., 2003. Atomic modelling of strengthening mechanisms due to voids and copper precipitates in α-iron. Philos. Mag. 83 (31–34), 3623–3641.
Schwarz, K.W., 1999. Simulation of dislocations on the mesoscopic scale. i. Methods and examples. J. Appl. Phys. 85 (1), 108–119.
Shin, C.S., Fivel, M.C., Verdier, M., Oh, K.H., 2003. Dislocation–impenetrable precipitate interaction: a three-dimensional discrete dislocation dynamics analysis. Philos. Mag. 83 (31–34), 3691–3704.
Shin, C.S., Fivel, M., Kim, W.W., 2005. Three-dimensional computation of the interaction between a straight dislocation line and a particle. Modelling Simul. Mater. Sci. Eng. 13, 1163–1173.
van der Giessen, E., Needleman, A., 1995. Discrete dislocation plasticity: a simple planar model. Modelling Simul. Mater. Sci. Eng. 3, 689–735.
Vogel, S.M., Rizzo, F.J., 1973. An integral equation formulation of three dimensional anisotropic elastostatic boundary value problems. J. Elast. 3 (3), 203–216.
Wang, Y.U., Jim, Y.M., Cuitino, A.M., Khachaturyan, A.G., 2001. Nanoscale phase field microelasticity theory of dislocations: model and 3D simulations. Acta Mater. 49, 1847–1857.
Xiang, Y., Cheng, L.-T., Srolovitz, D.J., Weinan, E., 2003. A level set method for dislocation dynamics. Acta Mater. 51, 5499–5518.
Zbib, H.M., Rhee, M., Hirth, J.P., 1998. On plastic deformation and the dynamics of 3D dislocations. Int. J. Mech. Sci. 40, 113–127.